Multi-fidelity Nonlinear Aeroelastic Analysis of a Strut-braced Ultra-high Aspect Ratio Wing Configuration

Peter Nagy *, Bryn Jones†, Edmondo Minisci‡, and Marco Fossati §
Aerospace Centre, University of Strathclyde, Glasgow, G1 1XJ, United Kingdom

Alvaro Cea ¶ and Rafael Palacios‖
Imperial College, London, SW7 2AZ, United Kingdom

Nicolas Roussouly**
Institute of Technology IRT Saint-Exupéry, 3 Rue Tarfaya, 31400 Toulouse, France

Nonlinear aeroelasticity of a strut-braced ultra-high aspect ratio wing aircraft is investigated using a multi-fidelity simulation environment. A baseline aeroelastic solver based on an unsteady vortex-lattice method and geometrically-exact composite beam model is coupled with a data-driven model order reduction tool based on high-fidelity aerodynamics. This provides sectional corrections, retrieved from a basis created using proper orthogonal decomposition, to the lower-order tools. Those corrections incorporate the three-dimensional and compressibility effects of the full strut-brace wing aircraft geometry and thus result in a computationally-efficient analysis framework suitable for multi-disciplinary design optimization. Verification of the reconstruction process is first presented, and the static and dynamic aeroelasticity of the strut-braced wing configuration are finally investigated.

I. Introduction

In the effort of minimizing environmental impact of aviation, aircraft designs with a significant increase in aerodynamic efficiency become desirable. Configurations with ultra-high aspect ratio wings (UHARWs) offer a promising avenue of development towards this goal. The overall improvement in performance is apparent as the L/D ratio is increased in contrast to conventional configurations and in-service aircraft. The inevitable increase in flexibility as the wing aspect ratio increases may pose some challenges regarding the interaction of disciplines traditionally decoupled and the appearance of nonlinear effects. As a consequence, aeroelastic analysis is set to dominate many aspects of the design. Additionally, structural problems may also arise; due to the increased wing bending moment some form of structural reinforcement becomes necessary. To cope with this, strut-braced wing (SBW) designs generated interest in the community (such as the well-known Boeing SUGAR concept [1]) as a solution that enables the use of UHARWs, noting that similar cantilever UHARW configurations with suitable structural properties would introduce substantial weight penalties, offsetting the gains in aerodynamic efficiency [2]. The strut-brace concept, first proposed by Pfenninger [3], alleviates the higher wing loading associated with larger wing span as well as enables lower thickness-to-chord ratio and sweep angle. It follows that the various drag contributions are thereby reduced, hence the increase in L/D when compared to an equivalent cantilever wing configuration [4].

That tradeoff between aerodynamic and structural efficiency becomes the defining feature of UHARW, and thus the study of SBW configurations has been the focus of numerous studies in multi-disciplinary design optimization (MDO) [4–6]. However, as noted in [2] the computational cost of solving high-fidelity Fluid-Structure Interaction (FSI) problems is very high, which is necessary to realize the aero-structural coupling. In the context of design optimization these costs become prohibitive: for example flutter analysis would necessitate solving an unsteady FSI problem. To

*PhD student, Department Mechanical and Aerospace Engineering, 75 Montrose street, AIAA Member.
†Postdoctoral Researcher, Department of Mechanical and Aerospace Engineering, 75 Montrose Street, G1 1XJ Glasgow, AIAA Member.
‡Associate Professor, Department of Mechanical and Aerospace Engineering, 75 Montrose Street, G1 1XJ Glasgow, AIAA Member.
§Associate Professor, Department Mechanical and Aerospace Engineering, 75 Montrose street, AIAA Member.
¶Research Associate, Department of Aeronautics, South Kensington Campus, SW7 2AZ
‖Professor of Computational Aeroelasticity, Department of Aeronautics, South Kensington Campus, SW7 2AZ, AIAA Associate Fellow.
**Research Engineer, Multidisciplinary Design Optimization Team.

This is an peer reviewed, accepted author manuscript of the following research paper: Nagy, P., Jones, B., Minisci, E., Fossati, M., Cea, A., Palacios, R., & Roussouly, N. (2022). Multi-fidelity nonlinear aeroelastic analysis of a strut-braced ultra-high aspect ratio wing configuration. In AIAA AVIATION 2022 Forum [2022-3668] American Institute of Aeronautics and Astronautics Inc, AIAA. https://doi.org/10.2514/6.2022-3668

facilitate optimization lower-fidelity tools can be used to solve the coupled aero-structural system. Fugate et al. [2] adopted a methodology where the low-fidelity aerodynamic solution is corrected using a sectional model that accounts for nonlinear transonic and viscous flow effects. In this work a methodology is introduced that leverages 3D CFD solutions for the aerodynamic correction but it is sufficiently fast to be used in MDO.

As established, optimization or other multi-query problems can present prohibitive costs, which holds true not only in the context of coupled aero-structural problems but also for purely aerodynamic problems, where three-dimensional flows around complex geometries are to be solved with high-fidelity CFD [7]. Similarly, to account for all conditions throughout the flight envelope an immense number of simulations must be performed, again driving costs to become prohibitive [8]. Model order reduction can offer accurate flow field predictions at greatly reduced cost [9]. The common driving methodology of the various model order reduction methods is the extraction of fundamental structures, which leads to a reduction in the dimensionality of the problem [10]. The Reducer Order Modelling (ROM) methodology within the multi-fidelity framework adopts an equation-free, purely data-driven approach. A set of high-fidelity flow solutions are computed to construct the low-dimensional model, which then allow for solution reconstruction elsewhere in the design space. An in-house tool is used for the aerodynamic ROM, called RAZOR [9, 11, 12].

The aeroelastic code used is SHARPy [13], whose basic solvers are a Unsteady Vortex Lattice Method (UVLM) for the aerodynamics, which is coupled to a geometrically-exact composite beam model (GEBM) for the primary structural components. This approach can capture arbitrarily large wing deformations, within the assumptions of potential-flow theory. Analytical linearizations of both structural and aerodynamic equations about nonlinear equilibrium conditions also enable the effect of wing deformations in flutter and other dynamic characteristics of the vehicle [14]. Sectional steady corrections have been recently incorporated on the baseline aerodynamic solver [15].

In addition to RAZOR and SHARPy, several open-source tools have been used in order to implement the whole framework, such as GEMSEO [16], CPACS [17] along with Tigl [18]. GEMSEO is a generic engine for MDO. It enables to automatically build MDO processes based on MDO formulations. In the current paper, its primary use is to integrate and orchestrate the various models (solvers) involved in the computation. CPACS is a common data definition for the air transportation system and enables to fully describe an aircraft configuration based on parameters. Finally, Tigl is a CPACS-related tool that brings several features for the model handling such as CAD generation of the fused model.

In summary, the objective of this work is present an analysis of an SBW configuration through a multi-fidelity framework that 1) is robust, 2) can produce aeroelastic studies that account for large excursions of the wing, and 3) is fast to be used in MDO. The aim of the an analysis is to show the impact of the corrections on the elastic solution when 3D flow effects are incorporated. The framework is multi-fidelity in the sense that the integrated tools are of varying fidelity and allow for incorporating effects from more accurately resolved flows through a data-driven aerodynamic Reduced Order Modelling (ROM) database. The configuration considered is a mid-range aircraft, with strut-braced UHARW, referred to hereafter as *SBWS*. The configuration is propagated from the conceptual design presented in [19]. The test case demonstrated here accounts only for two geometric design variables (span and sweep of the wing), but is devised in order to cope with much larger problems at the level of preliminary aircraft design.

The structure of the paper is as follows: an overview of the methodology is presented in Section II, describing the framework for the proposed multi-fidelity approach; in Section III the aeroelastic formulation of the problem is detailed; in Section IV more detail is provided on the model order reduction method adopted for this work; in Section V the demonstrated test case is described in detail as well as an overview of the mesh deformation and optimization step is given; in Section VI a set of verification exercises are presented; while in Sectio VII an aeroelastics study of the SBWS is shown; finally Section VIII contains concluding remarks and future outlook.

II. Methodology of Multi-fidelity Framework

In this section an overview of the multi-fidelity framework is given. It is necessary to clarify that in the context of this work *multi-fidelity* refers to the integration of differing fidelity tools, and the ability to improve the accuracy of the aeroelastic analysis through the aerodynamic ROM. As discussed in section I it is desirable to develop methods that allow for solutions to be obtained in an accurate but fast manner. This allows for use in an MDO context, relevant for the

design of an SBW configuration. With the methodology introduced here aeroelastic analyses can be provided for any new geometry of a given configuration (within some bounds defined a-priori).

Since the aerodynamic ROM requires an ensemble of CFD solutions, the framework can be separated into an offline and online stage. The offline stage consists of a Design of Experiments (DoE) and mesh generation step, followed by CFD to construct the ROM. The online stage stage allows to predict the aero-elastic solution of a new geometry using 3D flow reconstruction from the ROM as a correction to the lower-order aerodynamic model. It is crucial for both stages to generate the geometry in a consistent way with respect to the models. This is ensured through the use of a dedicated GEMSEO/CPACS interface along with Tigl which enable to generate 3D CAD models as an input to the mesh generation and to update/generate a mid-fidelity aero-structural model for the online stage. An overview of the steps involved in each stage are given here. The offline stage consists of the following steps:

1) **Design of Experiments (DoE).** Design variables are defined for a given problem and the resulting design space is sampled. For this work the design space consists only of geometrical parameters, specifically semi-span and sweep angle of the wing but the framework can accommodate many more variables, noting the inevitable increase in offline costs. The design space must be sampled in such a way so that the flow physics is sufficiently captured across all sampled points.
2) **Mesh generation.** As the geometry varies across the design space a separate mesh is required for each point. However, a consistent mesh topology is necessary for the model order reduction step. To achieve this an initial mesh is generated for the *baseline configuration* resulting from conceptual design. Then all other meshes are obtained by deforming the baseline mesh. This is realized with the deformation module of SU2 [20] combined with an optimization approach that minimizes the distance between the deformed mesh and the corresponding CAD model of a particular geometry.
3) **CFD simulations.** Flow solutions are computed for each geometry that correspond to points sampled during the DoE. For each point a set of simulations are executed for a range of angles of attack (AoA). This is required to facilitate the corrections in later steps.
4) **Construction of ROM.** The ensemble of flow solutions (snapshots) obtained in the previous step comprise the training set used for generating the aerodynamic ROM. To construct the low-dimensional model only the surface solution on the wing is used for this work. Note how the total number of snapshots will be a multiple of the initially sampled points (geometries). The resulting ROM database is used in the online stage to compute reconstructions, i.e. solutions referring to new geometries.

For the online stage, in addition to the GEMSEO/CPACS interface used for model generation, the underlying solvers of the overall process have all been wrapped into GEMSEO disciplines and connected together as a chain. This chain is finally seen as a standalone discipline which includes all steps described in the following and a schematic shown in Fig. 1:

1) **Model generation.** A parametric description of the model is stored in CPACS. Design variables (span and sweep) serve as inputs to the online process. The GEMSEO/CPACS interface allows for a consistent modification of the geometry by adjusting relevant parameters in CPACS, propagated from the input design variables. In combination with Tigl, this GEMSEO/CPACS interface is used to compute the wingbox based on the wing profile at sections and obtain the resulting properties for the structure. Tigl is also employed to provide the reference values of the wing planform.
2) **Reconstruction of target solution with RAZOR.** The aerodynamic ROM is used to reconstruct solutions for a new geometry defined by the design variables. Surface quantities of pressure and shear-stress as well as the new geometry are computed through the ROM for a range of AoA. The resulting 3D surface solutions are post-processed to compute sectional polars of aerodynamic coefficients at the location of the beam nodes defined in the previous step. The polars refer to 2D airfoils obtained directly from the 3D surface.
3) **SHARPy in rigid mode.** To facilitate the corrections, the slopes of polars must be obtained separately from SHARPy. It is executed at two AoA with no elasticity included, which allows to compute deltas with respect to the values computed through RAZOR.
4) **Nonlinear aeroelastic simulations.** The aerodynamic solver employs an unsteady vortex lattice method (UVLM). The forces resulting from the UVLM part are then corrected so that higher-order effects of the flow are incorporated into this method. The loads are then transferred onto a geometrically exact composite beam model (GEBM) describing the structure.

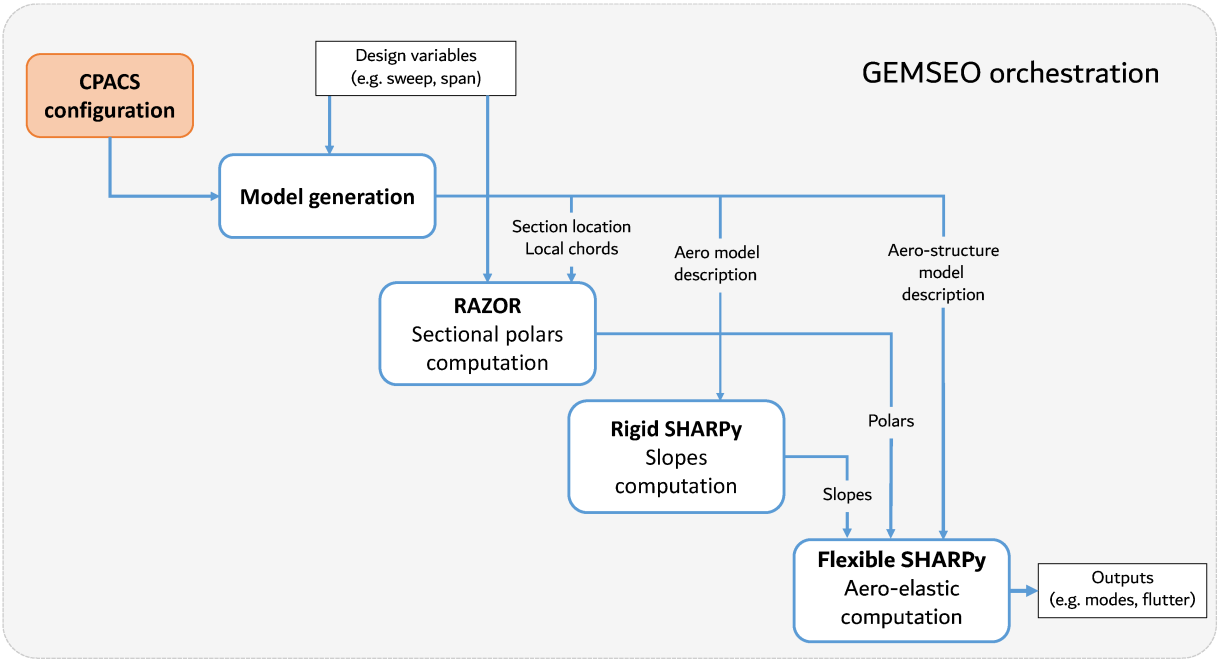

Fig. 1 Schematic outlining the procedure of the aeroelastic analysis framework.

III. Aeroelastic formulation

The full aeroelastic system is formed by coupling a GEBM formulation [21, 22] with the UVLM [23] and linearizing around arbitrary configurations. This has been implemented into the code SHARPy [13], a modular framework for aeroelastic computations.

In its basic form the solver computes static (trim) or dynamic simulations on the geometrically-nonlinear equations on free-flying vehicle. Once a nonlinear equilibrium is found, a linearized analysis can be carried out small perturbation of the equations. Let $\boldsymbol{\eta}$ be the perturbed elastic DoF of the beam around an equilibrium $\boldsymbol{\eta}_0$, $\boldsymbol{\beta}$ the perturbed rigid-body dynamics, and $\boldsymbol{N}_\eta$, $\boldsymbol{N}_\beta$ the corresponding incremental external forces on the structure:

$$\boldsymbol{\mathcal{M}}(\boldsymbol{\eta}_0)\begin{bmatrix}\ddot{\boldsymbol{\eta}}\\ \ddot{\boldsymbol{\beta}}\end{bmatrix} + \boldsymbol{C}(\boldsymbol{\eta}_0,\dot{\boldsymbol{\eta}}_0,\boldsymbol{\beta}_0)\begin{bmatrix}\dot{\boldsymbol{\eta}}\\ \dot{\boldsymbol{\beta}}\end{bmatrix} + \boldsymbol{\mathcal{K}}(\boldsymbol{\eta}_0,\dot{\boldsymbol{\eta}}_0,\boldsymbol{\beta}_0)\begin{bmatrix}\boldsymbol{\eta}\\ \boldsymbol{0}\end{bmatrix} = \begin{bmatrix}\boldsymbol{N}_\eta\\ \boldsymbol{N}_\beta\end{bmatrix} \tag{1}$$

Similarly a linearization of the UVLM is sought as in [14], which yields a discrete, linear time invariant (DLTI). The bound and wake perturbation vorticity, $\boldsymbol{\Gamma}$, $\boldsymbol{\Gamma}_w$, are solved by imposing the non-penetration boundary condition at the bound lattice,

$$\boldsymbol{\mathcal{A}}\boldsymbol{\Gamma}^{n+1} + \boldsymbol{\mathcal{A}}_w\boldsymbol{\Gamma}_w^{n+1} = \boldsymbol{\mathcal{B}}\boldsymbol{u}_a^n \tag{2}$$

where $\mathbf{u}_a$ is the input vector to the aerodynamics containing the perturbation to the aerodynamic grid points and any external atmospheric disturbance. The propagation of the wake downstream is modelled by enforcing the Kutta-Joukowski condition. The aerodynamic forces, that enter Eq. (1) in $\boldsymbol{N}$ after linearization, are concatenated in the output vector $\boldsymbol{y}_a$; the aerodynamic state vector is assembled as $\boldsymbol{x}_a^n = [\boldsymbol{\Gamma}^n; \boldsymbol{\Gamma}_w^n; d\boldsymbol{t}\boldsymbol{\Gamma}^n; \boldsymbol{\Gamma}^{n-1}]^\top$, and the final DLTI aerodynamic system is:

$$\begin{aligned}\boldsymbol{x}_a^{n+1} &= \boldsymbol{A}\boldsymbol{x}_a^n + \boldsymbol{B}\boldsymbol{u}_a^{n+1}\\ \boldsymbol{y}_a^{n+1} &= \boldsymbol{C}\boldsymbol{x}_a^n + \boldsymbol{D}\boldsymbol{u}_a^n\end{aligned} \tag{3}$$

A similar state-space system is realized for the structural description around a nonlinear equilibrium and both are coupled such that the aerodynamic forces from the output of the aerodynamic system (forces) enter the structural system, and similarly this system outputs the displacements and velocities to the aerodynamics. The aerodynamic corrections from high fidelity data have to be then applied to 1) the tightly coupled simulation that finds the nonlinear equilibrium of the aircraft; and 2), to the matrix $\boldsymbol{A}$ in the aerodynamic state-space system for the unsteady affects and to the vector $\boldsymbol{y}_a$ as a scaling of the forces. The focus in this work is on the correction of the nonlinear aeroelastic equilibrium, which will be described in the next section.

A. Nonlinear framework for design

The ultimate objective of the proposed solution is to perform design and optimization analysis in a reliable yet efficient manner, for which the strategy depicted in Fig. 2 has been implemented. A set of parameters determine the aircraft geometry from which a reduced order model library has been generated with RAZOR. The structural model and the underlying lifting panels from the geometry are passed onto SHARPy which builds the aeroelastic model and runs the simulation. At each evaluation point the nonlinear equilibrium of the configuration is found in a tightly coupled iteration where the UVLM forces are corrected with the sectional aerodynamic polars before being transferred to the structure. The aeroelastic system is linearized around the equilibrium obtained at the prescribed flight condition, with the linearized UVLM also enhanced from the ROM library. The static aeroelastic loads are retrieved from the equilibrium and the resulting state-space system is used to compute dynamic loads and stability of the configuration.

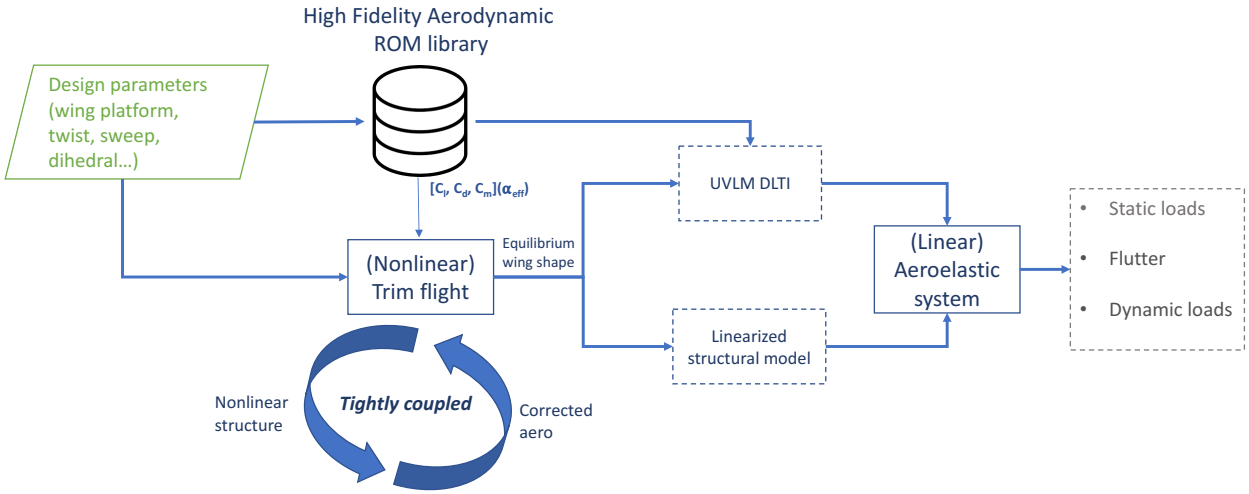

Fig. 2 Schematic of the proposed aeroelastic solution

The correction process in the calculation of the nonlinear equilibrium is outlined as follows:

1) Build UVLM rigid aerodynamic coefficients.
2) Iterate to find nonlinear aeroelastic equilibrium:
    1) Compute the UVLM aerodynamic forces and their corresponding aerodynamic coefficients.
    2) Map the coefficient of lift given by the panel method, C_l^{in}, to an effective AoA, α_{eff}, for each section along the lifting surfaces using the loads on the rigid model (C_{l0}^r and $C_{l\alpha}^r$ for the 0 AoA and lift slopes respectively):

$$\alpha_{eff} = \frac{C_l^{in} - C_{l0}^r}{C_{l\alpha}^r} \tag{4}$$

    3) Using α_{eff}, obtain the high fidelity coefficients, C_n^{out}, via interpolation in the high fidelity database. This process is depicted in Fig. 3
    4) Replace the UVLM aerodynamic forces with those corresponding to the high fidelity data.
    5) Transfer the aerodynamic loads to the structure and check convergence to repeat the loop or continue onto building the linearized dynamical system.

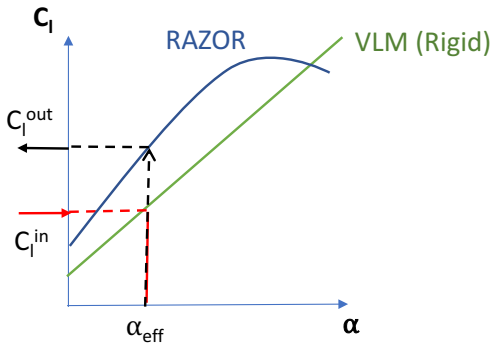

Fig. 3 Calculation of effective angle of attack from sectional loads

IV. Reduced Order Modelling Framework

RAZOR, the aerodynamic ROM tool consists of an offline stage and an online stage, largely corresponding to the steps details in section II. The low-dimensional model is built after DoE within the offline stage, whereas new solutions are reconstructed in the online stage. In this section more detail is given about the POD-based method employed in the framework.

POD is a linear model order reduction method. The algorithm is used to extract orthogonal basis functions (or POD modes) from *snapshots*, referring to the method adopted for the basis extraction as introduced by Sirovich [24]. Model order reduction of the system is achieved if sufficiently few fundamental structures characterize the dynamics. Sirovich's method of snapshots demonstrates that POD modes can be expressed as a linear combination of snapshots:

$$\phi(\mathbf{x}) = \sum_{i=1}^{N_s} b_i \mathbf{u_i} \tag{5}$$

where ϕ is the POD mode, $\mathbf{u_i}$ is the vector of the quantity of interest across all grid points of the mesh, N_p for snapshot i and b_i is the associated coefficient [24]. The coefficients can be obtained by the solution of an eigenvalue problem [10] as follows:

$$\mathbf{R}\mathbf{b}_i = \lambda_i \mathbf{b}_i \tag{6}$$

where $\mathbf{R}$ is the cross-correlation matrix of the snapshot matrix $\mathbf{U} = \{\mathbf{u}_1, \mathbf{u}_2, ..., \mathbf{u}_{N_s}\}$, defined as $\mathbf{R} = \mathbf{U}^T\mathbf{U}$. The energy associated with each mode is given by the eigenvalues λ_i, in essence quantifying the relative importance of a mode [25]. Thus, the modes can be ordered according to their energy content and truncated based on a threshold energy content. Since the number of DoF in the low-dimensional model is given by the number of POD modes, an efficient order reduction is achieved in this way [9]. The normalized POD modes are expressed as:

$$\phi_i = \frac{1}{\sqrt{\lambda_i}} \mathbf{U}\mathbf{b}_i \tag{7}$$

where $\sqrt{\lambda_i}$ is the normalization factor.

A reconstructed solution is expressed as a linear combination of the POD modes and their associated coefficients, a_i. The coefficients are obtained by way of Radial Basis Function (RBF) interpolation. Then a reconstructed solution is computed as:

$$\mathbf{u}(\mathbf{x}) \approx \hat{\mathbf{u}} = \sum_{i=1}^{N_m} a_i \phi_i(\mathbf{x}) \tag{8}$$

V. Problem Definition

The problem used to demonstrate the framework is described in this section. The SBWS configuration as referred to in section I is described by two parameters, the semi-span of the wing and the sweep angle. Hence, the design space is two-dimensional and the sampling is shown in Fig. 4. Flow solutions of 12 distinct geometries comprise the training set for the aerodynamic ROM database and the multi-fidelity framework is expected to work reliably within the bounds of this parameter space. Note however that the aerodynamic ROM is constructed using 72 snapshots, to facilitate the corrections described in sections II and III. This means that for every geometry 6 solutions are obtained at varying AoA, in the range of $-10°$ and $15°$ with $5°$ increments. Solutions are always reconstructed at these angles, i.e. there is no enrichment. The *baseline configuration* mentioned in Section II is not part of this training set, instead it is an example geometry used in the verification exercises and to demonstrate elastic results.

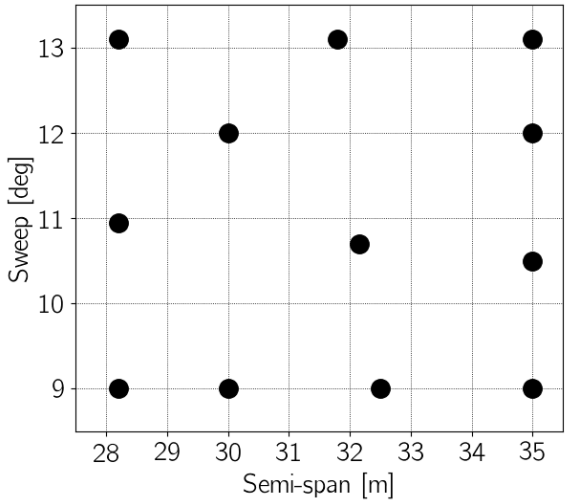

Fig. 4 Twelve points sampled from the two-dimensional design space of semi-span and sweep.

The geometry is defined within CPACS. As explained in section II the GEMSEO/CPACS interface allows to generate a new configuration for each sampled DoE point in a consistent way such that the full parametric description is affected by the design variables: semi-span and sweep of the wing. For example the orientation and dimensions of the strut also change based on the inputs. A *fused* 3D CAD model of the aircraft half-body is created using Tigl. From this an unstructured mesh is generated for the baseline configuration, with a semi-span of 31 m and sweep of 12.5°. The mesh consists of 2,074,673 elements and 426,587 grid points. The surface mesh itself is shown in Fig. 5 with the various components annotated.

The aerodynamic problem considers inviscid flow over the aircraft surface. To obtain the flow solutions the CFD solver of SU2 [20] is used. The numerical scheme employed is Roe. The flight conditions correspond to cruising flight at an altitude of 11 km. Freestream values are shown in table 1.

Mach number	Temperature (K)	Pressure (Pa)
0.745	218.6	22,700

Table 1 Freestream conditions for the MR-SBWS in cruising flight.

To illustrate the flow over the SBWS aircraft in Fig 6 an example C_p distribution is shown, presenting the flow features such as transonic shocks over the suction side of the wing as well as on the strut. Note that only the relevant surfaces are processed of the CFD solutions. In this work this is restricted only to the wing.

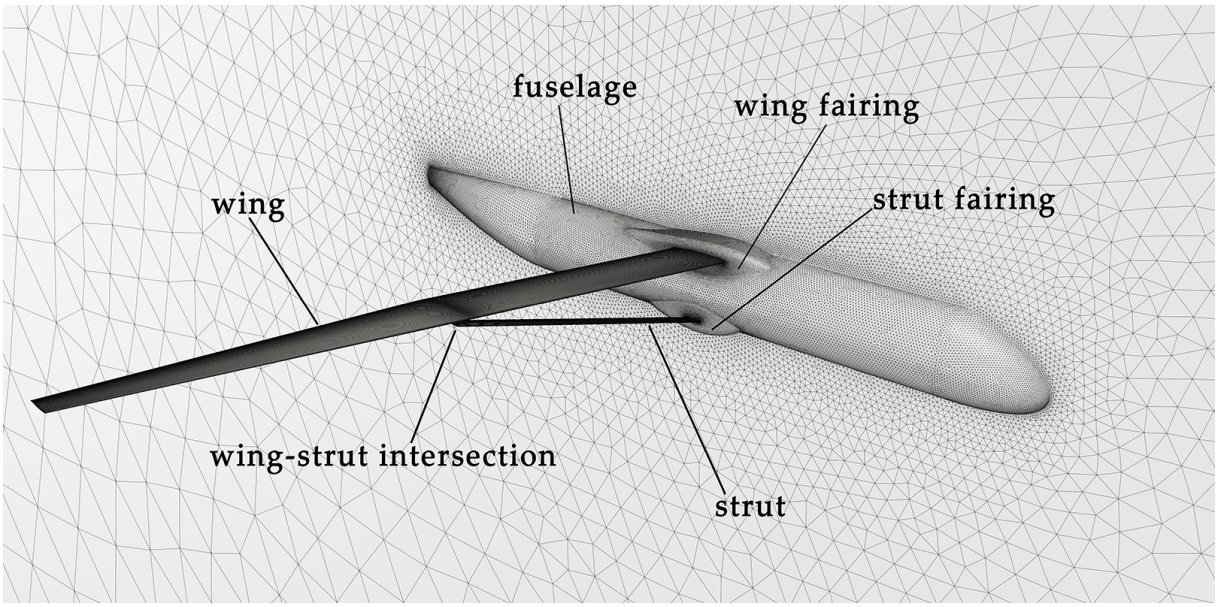

Fig. 5 Surface elements of the baseline mesh, annotated with important features of the MR-SBWS. The geoemtry has a semi-span of $31m$ **and a quarter-chord sweep of** $12.5°$**.**

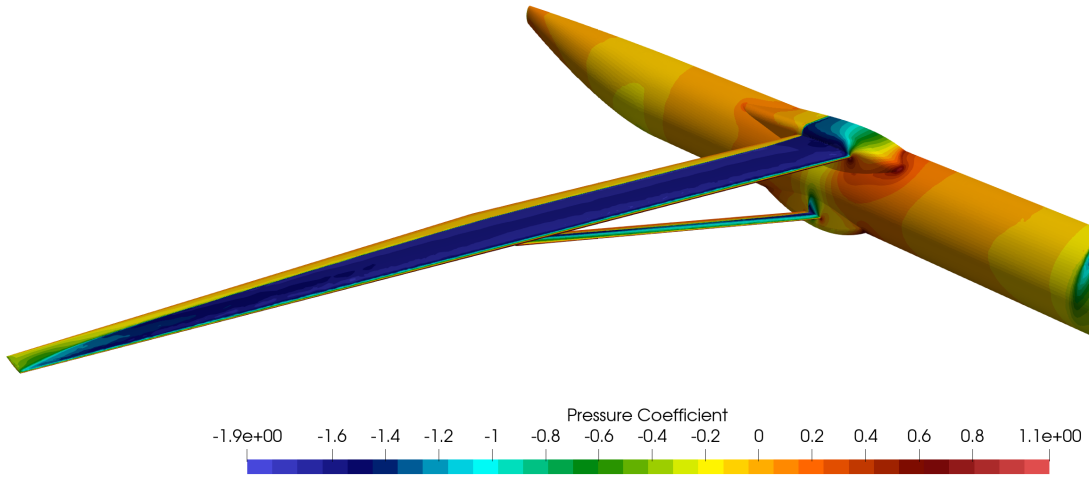

Fig. 6 Coefficient of pressure distribution over SBWS at $\alpha = 5°$ **for a configuration with a semi-span of** $35m$ **and sweep of** $12.0°$**.**

The structural model is described by beam elements and a number of beam nodes. Structural properties are computed from the wingbox. The wingbox is computed in relation to the structural beam nodes and it is illustrated in Fig. 7.

Only a preliminary version of the structural model has been tested and further work will look into improving this part of the configuration. The aeroelastic model is then composed of equivalent beam elements, distributed mass and aerodynamic panels as shown in Fig. 8.

A. Mesh Deformation and Optimization

As outlined in section II the DoE is followed by a mesh deformation stage. To compute an appropriate low-dimensional model a consistent mesh topology is required across all the snapshots, which follows from the snapshot-based POD formulation described in section IV. As the design space consists of geometrical parameters, a consistent topology (with respect to the number of grid points and connectivity) cannot be ensured if a distinct unstructured mesh is generated for

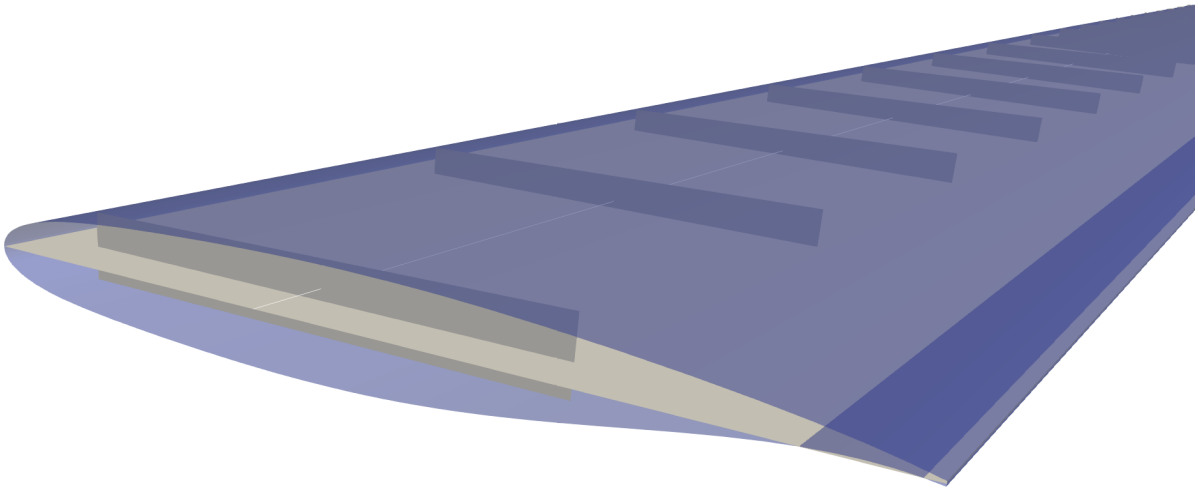

Fig. 7 Overlay of the wingboxes at sections (obtained from Tigl) and the 3D geometry of the wing.

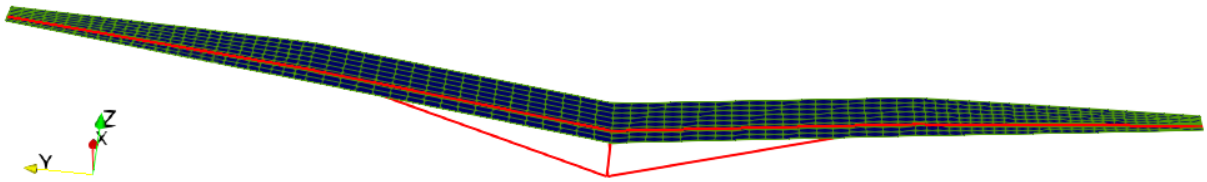

Fig. 8 Reference SBW aeroelastic model

each geometry. To cope with this circumstance all meshes are propagated from an initial baseline mesh shown in Fig. 5. To achieve this the mesh deformation module of SU2 is used.

The deformation is performed by defining a free-form deformation (FFD) box enclosing the wing, and applying displacements to the nodes of the box. The SU2 deformation module then linearly interpolates the box displacements onto the grid points of the mesh.

An optimization approach, managed through GEMSEO, is used to deform the mesh to match the desired geometry, where the objective function is measured by the distance between certain points on the mesh, and certain corresponding points on an independently generated CAD model obtained through the GEMSEO/CPACS interface. In order for the optimization to be efficient, a reduced form of the baseline mesh is created that contains only the mesh points relating to the objective function. The optimization itself is performed on this reduced mesh, then the results from this optimization are used to deform the full mesh. An example of a resulting *deformed mesh* is shown in Fig. 9.

Since the FFD box cannot be aligned exactly with the curved root-fairing intersections for both the wing and the strut, any deformation applied to the tip of the wing also deforms the root, either causing a discontinuity in the mesh or changing the shape of the fairing. When optimization constraints are applied that limit the translation of the root, the objective is not reduced satisfactorily, instead the minimization of the translation of the root is treated as a separate optimization problem performed after the desired sweep/span/etc. at the tip is achieved.

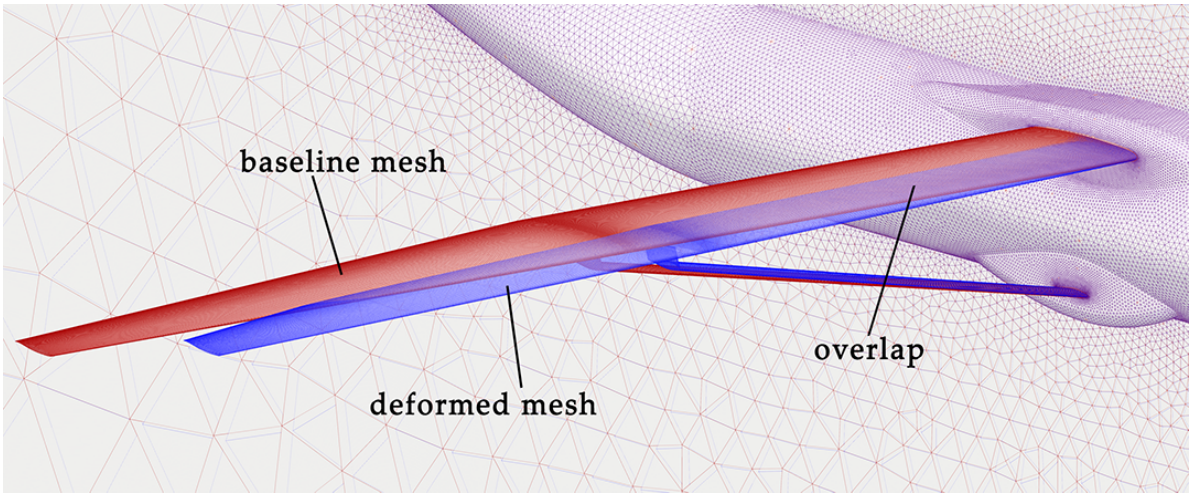

Fig. 9 Baseline mesh (red) superimposed with a deformed mesh (blue). Here the baseline mesh has a semi-span of 31 **metres and a quarter-chord sweep angle of** 12.5°**, while the deformed mesh has a semi-span of** 25 **metres and** 9° **sweep, with no other changes in the parameters.**

VI. Verification

To verify that the corrections are applied appropriately within the framework, the polars of aerodynamic coefficients are obtained from SHARPy that correspond to the full 3D wing surface. To consider the process verified, the polars must match (within some tolerance) those that are obtained directly from the reconstructed solutions computed with RAZOR. To achieve this, SHARPy is run so that the structure is infinitely rigid; only aerodynamics is present. To demonstrate this three exercises were done, where C_L and C_D are compared.

The first exercise is associated with a geometry that is part of the training set. Since all POD modes are used in the reconstruction as explained in Section IV the reconstruction must match the original CFD solution exactly. Polars are compared in Fig. 10. As expected the curves obtained from SU2 and RAZOR are exactly superimposed, but some discrepancy can be observed when comparing the results of SHARPy, most apparent at higher AoA. This can be attributed to interpolation steps when extracting sections from the 3D flow solution as well as interpolation between polars along the span in SHARPy. This is needed as nodes are placed between section in SHARPy. The $C_D - \alpha$ curve shows very good agreement with the reference values.

The second exercise is associated with the baseline geometry. Additional CFD solutions are also available for this point which will allow to contrast the discrepancies between the reference polars coming from RAZOR, the polars obtained from SHARPy, and those coming directly from CFD, noting also the differences observed in the first exercise. The polars are compared in Fig. 11. There is a visible discrepancy at the two extreme AoA when the reconstruction is compared to the reference CFD solutions, indeed these inaccuracies are much larger than any difference between the two polars being verified. This may be attributed to the fact that the reconstructions are on the boundary of the ROM's parameter space. It follows that any errors arising during the correction process are similar or smaller than those resulting from the reconstruction.

The final exercise is aimed to demonstrate the same behaviour throughout the whole parameter space which is achieved by performing a parametric analysis. The results shown refer to the error over the whole parameter space for each discrete AoA. The error is evaluated for 49 uniformly sampled points in total, and an estimate of the error for the whole parameter space is obtained by way of interpolation. Figures 12, 13, and 14 show the errors over the parameter space. In some regions consistently higher errors can be observed which is to be investigated in future work.

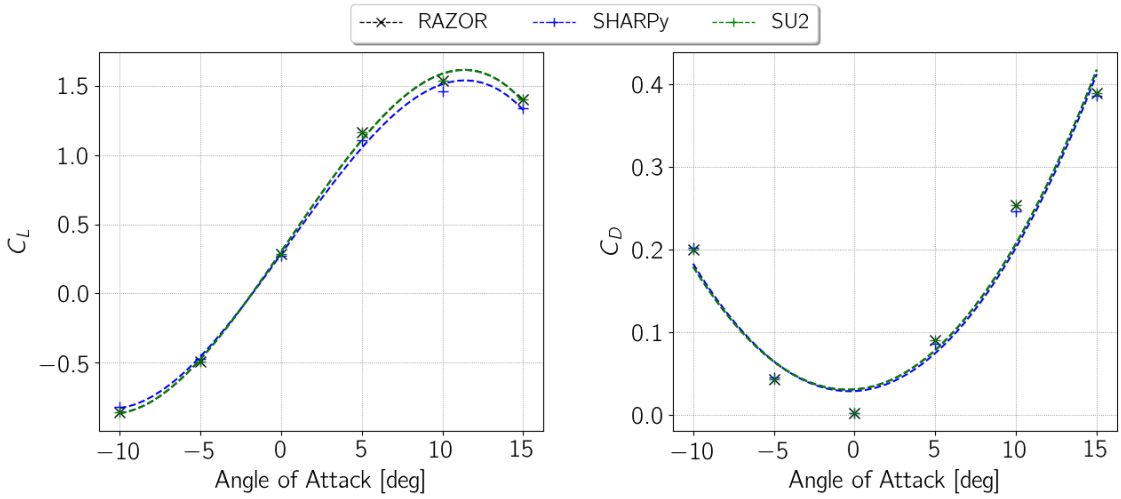

Fig. 10 Polars of C_L and C_D obtained from SHARPy are compared to the reference values obtained from RAZOR. The geometry has a semi-span of 35 m and sweep of 9.0°, and is part of the training set. The solution is exactly reconstructed in comparison to the CFD solution whose polars are also shown.

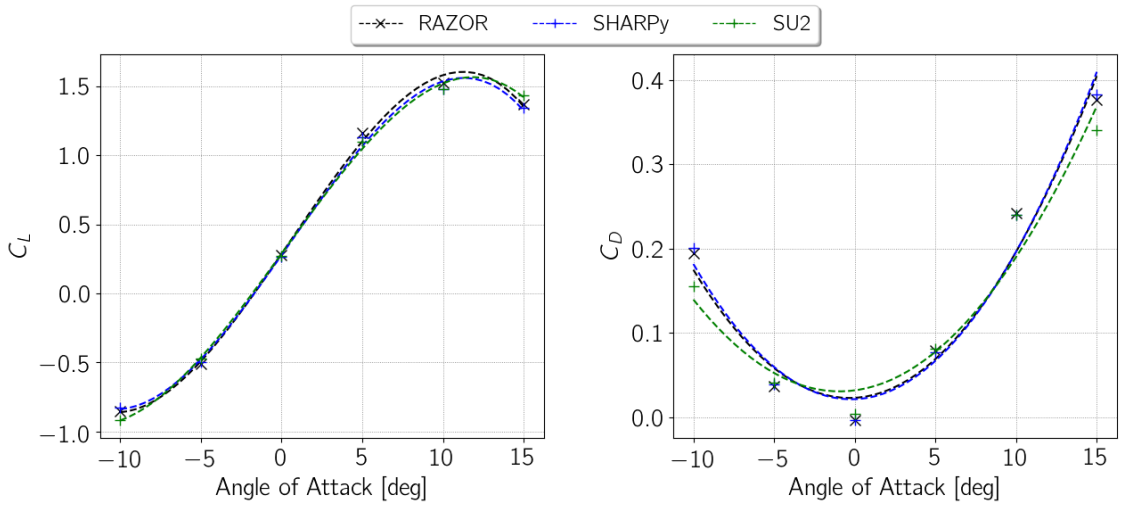

Fig. 11 Polars of C_L and C_D obtained from SHARPy are compared to the reference values obtained from RAZOR. Corresponds to the baseline geometry with a semi-span of 31 m and sweep of 12.5°, which is the baseline geometry. Curves obtained directly from CFD are also shown, illustrating the error in the reconstruction.

VII. Aeroelastic study of the SBWS configuration

Some preliminary aeroelastic results with and without the high fidelity corrections are presented in this section. The flow conditions are flow speed of $U_\infty = 219.9\ m/s$ and density $\rho = 0.365$ Kg/m^3. Fig. 15 presents the aeroelastic equilibrium of the wing using the standalone aerodynamics of the UVLM (in green) with the wake panels represented, and the corrected aerodynamics from RAZOR (in blue). The increase in the aerodynamic loading in the corrected model generates larger displacements on the wing. These come from higher order effects not captured by the VLM, including compressibility effects and the cambering of the laminar airfoils, which, although possible, was not including in the geometric definition of the panels.

To quantify the changes in the aerodynamic loading from the corrections, Fig. 16 presents the lift distribution normalized with the dynamic pressure along the wing span for the wing at 4 deg angle of attack. The figure includes

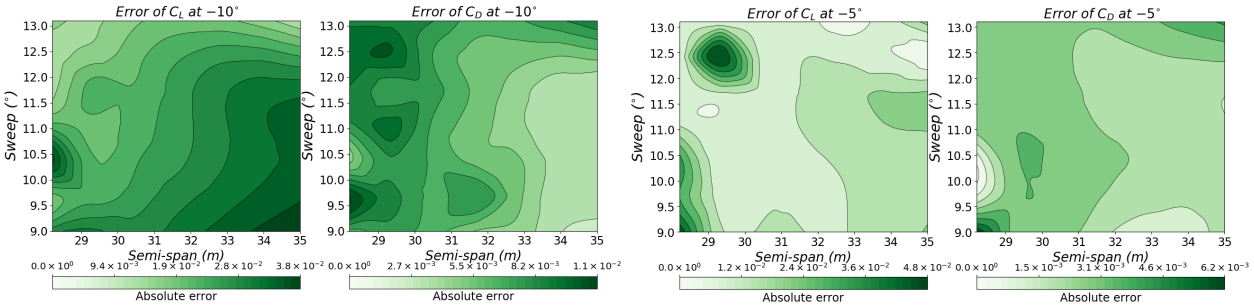

Fig. 12 Direct error in aerodynamic coefficients throughout the parameter space. Absolute value is shown. $\alpha = -10^\circ$ (left) and $\alpha = -10^\circ$ (right)

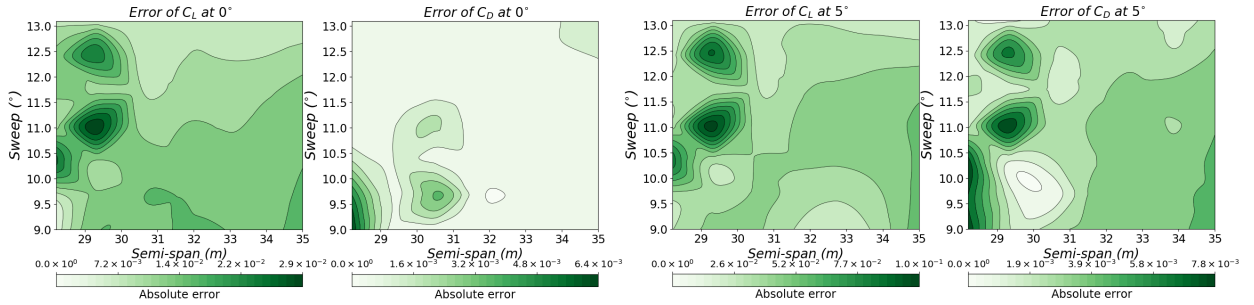

Fig. 13 Direct error in aerodynamic coefficients throughout the parameter space. Absolute value is shown. $\alpha = 0^\circ$ (left) and $\alpha = 5^\circ$ (right)

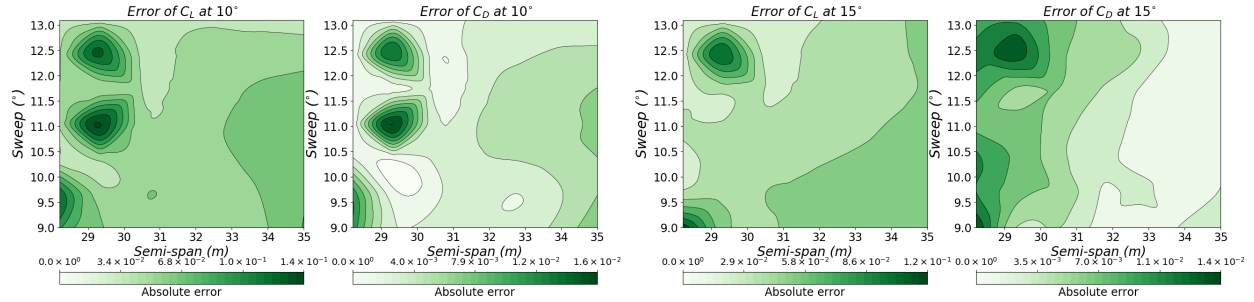

Fig. 14 Direct error in aerodynamic coefficients throughout the parameter space. Absolute value is shown. $\alpha = 10^\circ$ (left) and $\alpha = 15^\circ$ (right)

the lift on the deformed wing with and without the corrections. The loads on the rigid wing are also included. The high-fidelity corrections increases the loads up to around 50% at the wing root, and also capture more complex details on the inner wing and around the strut. Further work will include a more detailed study of these effects and their influence in the aeroelastic calculations.

Using an initial estimation of the distribution along the wing and the strut, the dynamics of the wing can now be explored. For that purpose, the linearized aeroelastic system is built around each equilibrium point and it is then written in state-space form, as described in Fig. 2. Fig. 17 shows the four modal shapes of the wing equilibrium around 0 and 4 degrees AoA. They are shown in dark and light blue, respectively. While the first bending mode is barely affected, and the different shapes in the plots are mostly due to normalization, there is a substantial increase in the natural frequencies of the second bending mode, which is involved in the flutter mechanism for this wing. Note that instead of a symmetric model, a left wing is added to the model, which introduces antisymmetric modes to the system.

Flutter results for 3 nonlinear equilibrium points are finally shown in Fig. 18. As observed above, the second bending

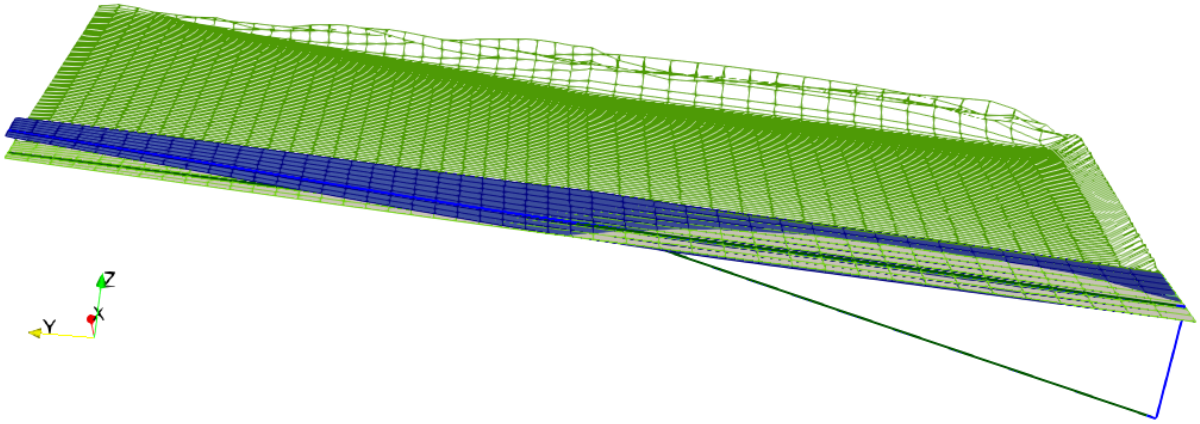

Fig. 15 SBW aeroelastic equilibrium with (blue) and without (green) corrections at 4 deg angle of attack

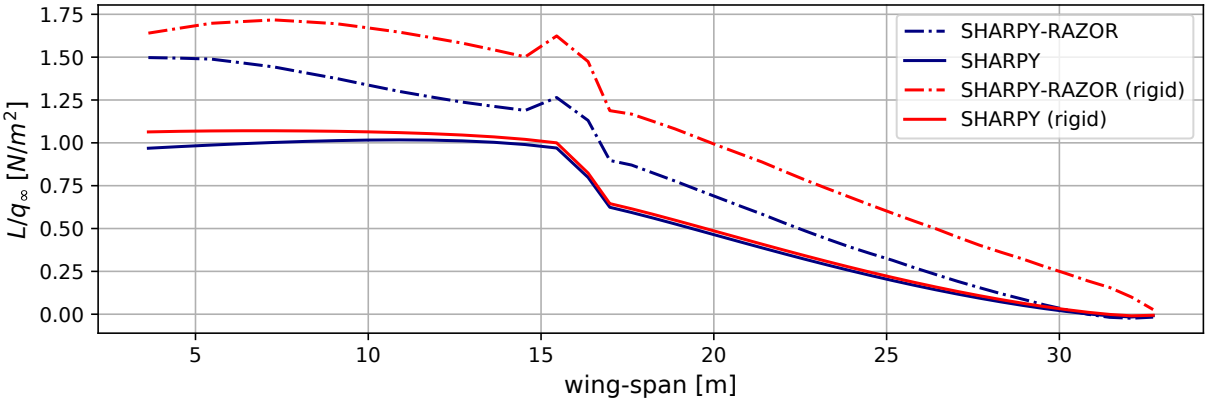

Fig. 16 Lift distribution for a rigid and elastic SBW at 4^o AoA

mode is strongly affected by the wing deformations, and therefore an important decrease in the flutter speed has been observed with the angle of attack. While such reduction in flutter speed is known to occur for high-aspect-ratio wings [26], this very reduction is likely to be an artifact of the particular mass distribution considered in this work. A more in depth analysis still needs to be carried out to understand the instability mechanisms in this wing, the sensitivity with modelling details, particularly with respect to the strut geometry, and the contribution of the aerodynamic corrections to the solution.

VIII. Concluding Remarks

In this paper a multi-fidelity framework was introduced that allows for nonlinear aeroelastic analysis in a fast but accurate manner, with the aim to be used in MDO. A mid-fidelity aeroelastic tool is coupled with an aerodynamic ROM tool based on high-fidelity CFD solutions. The latter provides corrections to the aerodynamics of the aeroelastic tool in the form of sectional polars. This methodology allows for keeping computational costs low. Indeed the dominant expense in terms of computations comes from the requirement to obtain an ensemble of high-fidelity CFD solutions to construct the aerodynamic ROM. The use of the framework has been demonstrated and verified using a highly relevant test case, specifically a strut-braced ultra-high aspect ratio wing configuration. This configuration is particularly well suited for this framework: the design of such aircraft necessitates the use of MDO, and presents a problem where there is a strong aero-structural coupling and aeroelastic effects are substantial.

Preliminary aeroelastic results have been presented using the proposed method. Further work is still necessary to assess the quality of the corrections under strong aeroelastic effects. For that purpose, the equilibrium shapes will be

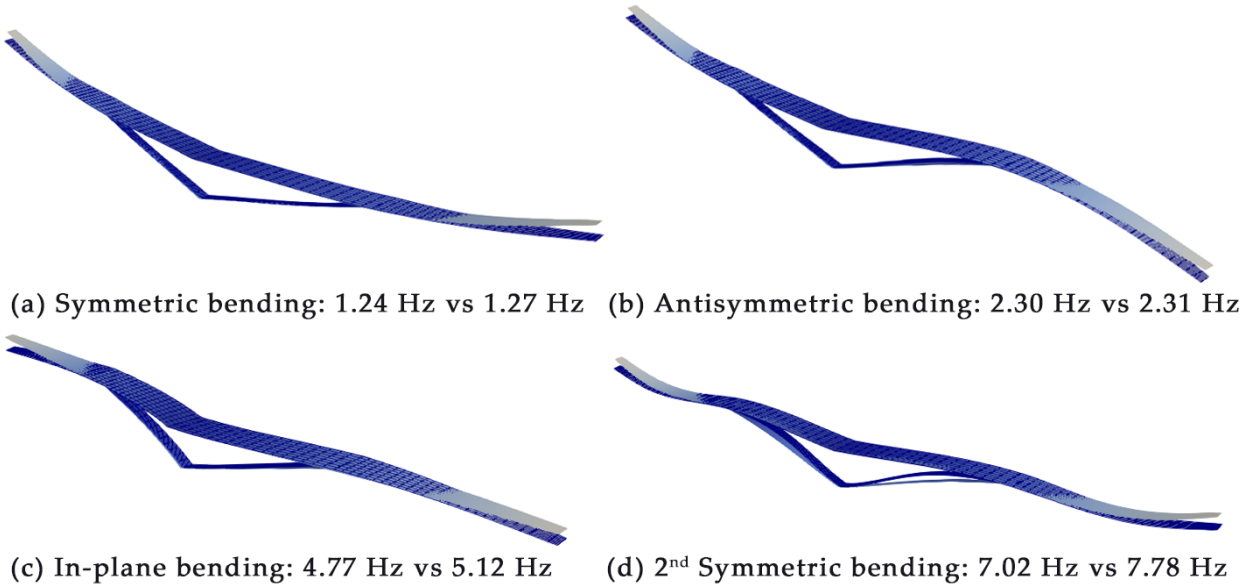

Fig. 17 Structural modes after aeroelastic equilibrium at 0 VS 4 deg AoA

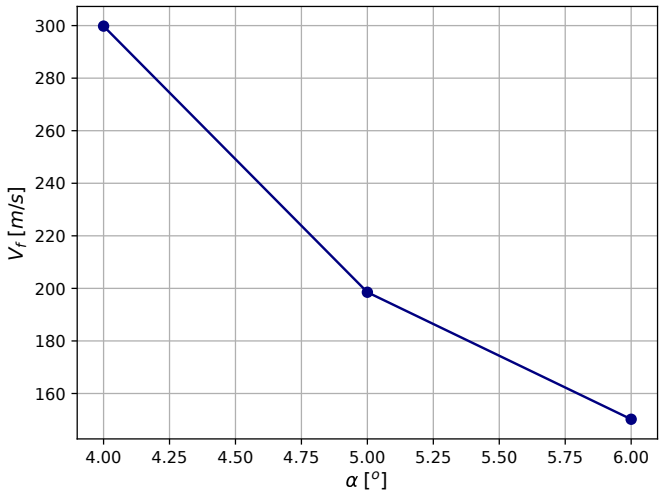

Fig. 18 Flutter speed at 4, 5 and 6 degrees AoA

retrieved and a high-fidelity CFD simulation will be carried out to obtain the actual expected force distribution.

The aerodynamic formulation of the problem can be extended to include viscous effects by solving for the Reynolds-averaged Navier-Stokes equations which would promote a much higher-fidelity ROM database. Considering specifically the aerodynamic ROM, more extensive sampling would increase the accuracy of reconstructions. Various methods can be introduced to find a good trade-off between offline computational expense and online accuracy, such as iterative sampling.

The presence of the strut is a critical aspect of the SBW configuration and the interference effects are substantial (see e.g. [2]). Therefore, in future work the strut aerodynamics must be considered as well, noting its effects are implicitly contained in the problem (as the solution on the wing surface is affected), but is not treated in the aeroelastic tool or contained in the ROM database.

Worthwhile future developments also include using the framework within MDO for a much higher dimensional problem, i.e. considering additional design variables in the parameter space. Note that offline costs are expected to increase by orders of magnitude as parameters are added. This is especially true if a good enough sampling of the parameter space is desired to be able to extract all the relevant physical content when creating the low-dimensional model. An important point must be mentioned with respect to the mesh deformation and optimization step adopted in this work. Further work with this approach revealed that the extension of the method for more complex geometries, such as the wing section shape, does not converge to a good solution. Increasing the number of control points in the FFD box was neither an efficient nor effective way of improving the convergence of this optimization. Assuming that a structured mesh is not an option, a specialized algorithm that directly deforms the mesh points according to each complex geometrical design parameter would need to be developed in order to solve this problem. To cope with this alternative approaches must be investigated that are less sensitive to the number of geometrical parameters, while still allowing for fast, automatic meshing of many geometries and allowing their use in the aerodynamic ROM.

Acknowledgments

The present work is part of a CleanSky2 project RHEA. RHEA has received funding from the Clean Sky 2 Joint Undertaking (JU) under grant agreement No 883670. The JU receives support from the European Union's Horizon 2020 research and innovation programme and the Clean Sky 2 JU members other than the Union.

References

[1] Bradley, M. K., and Droney, C. K., "Subsonic Ultra Green Aircraft Research: Phase I Final Report," Tech. Rep. NASA/CR–2011-216847, Boeing Research and Technology, 04 2011.

[2] Fugate, J., Nguyen, N., and Xiong, J., "Aero-Structural Modeling of the Truss-Braced Wing Aircraft Using Potential Method with Correction Methods for Transonic Viscous Flow and Wing-Strut Interference Aerodynamics," 2019. https://doi.org/10.2514/6.2019-3028.

[3] Pfenninger, W., "Laminar flow control laminarization. AGARD Spec. Course on Concepts for Drag Reduction," Tech. rep., 06 1977.

[4] Gur, O., Bhatia, M., Schetz, J., Mason, W., Kapania, R., and Mavris, D., "Design Optimization of a Truss-Braced-Wing Transonic Transport Aircraft," *Journal of Aircraft*, Vol. 47, 2010, pp. 1907–1917. https://doi.org/10.2514/1.47546.

[5] Grasmeyer, J., *Multidisciplinary Design Optimization of a transonic strut-braced wing aircraft*, ???? https://doi.org/10.2514/6.1999-10, URL https://arc.aiaa.org/doi/abs/10.2514/6.1999-10.

[6] Gundlach, J. F., Tetrault, P.-A., Gern, F. H., Nagshineh-Pour, A. H., Ko, A., Schetz, J. A., Mason, W. H., Kapania, R. K., Mason, W. H., Grossman, B., and Haftka, R. T., "Conceptual Design Studies of a Strut-Braced Wing Transonic Transport," *Journal of Aircraft*, Vol. 37, No. 6, 2000, pp. 976–983. https://doi.org/10.2514/2.2724, URL https://doi.org/10.2514/2.2724.

[7] Spalart, P., and Venkatakrishnan, V., "On the role and challenges of CFD in the aerospace industry," *The Aeronautical Journal*, Vol. 120, 2016, pp. 209–232. https://doi.org/10.1017/aer.2015.10.

[8] Ripepi, M., Verveld, M., Karcher, N., and al, "Reduced Order Models for Aerodynamic Applications, Loads and MDO," *CEAS Aeronaut J*, Vol. 9, 2018, pp. 171–193. https://doi.org/https://doi.org/10.1007/s13272-018-0283-6.

[9] Fossati, M., "Evaluation of Aerodynamic Loads via Reduced-Order Methodology," *AIAA Journal*, Vol. 53, 2015, pp. 1–17. https://doi.org/10.2514/1.J053755.

[10] Taira, K., Brunton, S., Dawson, S., Rowley, C., Colonius, T., McKeon, B., Schmidt, O., Gordeyev, S., Theofilis, V., and Ukeiley, L., "Modal Analysis of Fluid Flows: An Overview," *AIAA Journal*, Vol. 55, 2017. https://doi.org/10.2514/1.J056060.

[11] Pascarella, G., Fossati, M., and Barrenechea, G., "Model-based Adaptive Reduced Basis Methods for Unsteady Aerodynamics Studies," *AIAA Aviation 2019 Forum*, 2019. https://doi.org/10.2514/6.2019-3332, URL https://arc.aiaa.org/doi/abs/10.2514/6.2019-3332.

[12] Fortunato, G., Pascarella, G., Fossati, M., and Barrenechea, G., "Adaptive Reduced Order Modelling for Steady Aerodynamics Flows," *AIAA Scitech 2021 Forum*, 2021. https://doi.org/10.2514/6.2021-1748, URL https://arc.aiaa.org/doi/abs/10.2514/6.2021-1748.

[13] del Carre, A., Muñoz-Simón, A., Goizueta, N., and Palacios, R., "SHARPy: A dynamic aeroelastic simulation toolbox for very flexible aircraft and wind turbines," *Journal of Open Source Software*, Vol. 4, No. 44, 2019, p. 1885. https://doi.org/10.21105/joss.01885, URL https://doi.org/10.21105/joss.01885.

[14] Maraniello, S., and Palacios, R., "State-space realizations and internal balancing in potential-flow aerodynamics with arbitrary kinematics," *AIAA Journal*, Vol. 57, No. 6, 2019, pp. 2308–2321. https://doi.org/10.2514/1.J058153.

[15] Düssler, S., Goizueta, N., Muñoz-Simón, A., and Palacios, R., "Modelling and Numerical Enhancements on a UVLM for Nonlinear Aeroelastic Simulation," *AIAA SciTech 2022 Forum*, American Institute of Aeronautics and Astronautics, San Diego, California, USA, 2022. https://doi.org/10.2514/6.2022-2455.

[16] Gallard, F., Vanaret, C., Guénot, D., Gachelin, V., Lafage, R., Pauwels, B., Barjhoux, P.-J., and Gazaix, A., "GEMS: A Python Library for Automation of Multidisciplinary Design Optimization Process Generation," *2018 AIAA/ASCE/AHS/ASC Structures, Structural Dynamics, and Materials Conference*, 2018.

[17] Alder, M., Moerland, E., Jepsen, J., and Nagel, B., "Recent advances in establishing a common language for aircraft design with CPACS," 2020.

[18] Siggel, M., Kleinert, J., Stollenwerk, T., and Maierl, R., "TiGL: an open source computational geometry library for parametric aircraft design," *Mathematics in Computer Science*, Vol. 13, No. 3, 2019, pp. 367–389.

[19] Ma, Y., Karpuk, S., and Elham, A., "Conceptual design and comparative study of strut-braced wing and twin-fuselage aircraft configurations with ultra-high aspect ratio wings," *AIAA AVIATION 2021 FORUM*, 2021. https://doi.org/10.2514/6.2021-2425, URL https://arc.aiaa.org/doi/abs/10.2514/6.2021-2425.

[20] Economon, T. D., Palacios, F., Copeland, S. R., Lukaczyk, T. W., and Alonso, J. J., "SU2: An Open-Source Suite for Multiphysics Simulation and Design," *AIAA Journal*, Vol. 54, 2015. https://doi.org/https://doi.org/10.2514/1.J053813.

[21] Géradin, M., and Cardona, A., *Flexible multibody dynamics: A finite element approach*, John Wiley, Baffins Lane, Chichester, West Sussex, England, 2001.

[22] Hesse, H., Palacios, R., and Murua, J., "Consistent Structural Linearization in Flexible Aircraft Dynamics with Large Rigid-Body Motion," *AIAA Journal*, Vol. 52, No. 3, 2014, pp. 528–538. https://doi.org/10.2514/1.J052316, URL http://arc.aiaa.org/doi/abs/10.2514/1.J052316.

[23] Murua, J., Palacios, R., and Graham, J. M. R., "Assessment of wake-tail interference effects on the dynamics of flexible aircraft," *AIAA Journal*, Vol. 50, 2012, pp. 1575–1585. https://doi.org/10.2514/1.J051543.

[24] Sirovich, L., "Turbulence and the dynamics of coherent structures. I - Coherent structures. II - Symmetries and transformations. III - Dynamics and scaling," *Quarterly of Applied Mathematics*, Vol. 45, 1987. https://doi.org/10.1090/qam/910463.

[25] Bui-Thanh, T., Damodaran, M., and Willcox, K., "Aerodynamic Data Reconstruction and Inverse Design Using Proper Orthogonal Decomposition," *AIAA Journal*, Vol. 42, No. 8, 2004, pp. 1505–1516. https://doi.org/10.2514/1.2159, URL https://doi.org/10.2514/1.2159.

[26] Goizueta, N., Wynn, A., Palacios, R., Drachinsky, A., and Raveh, D. E., "Flutter Predictions for Very Flexible Wing Wind Tunnel Test," *Journal of Aircraft*, 2022. https://doi.org/10.2514/1.C036710, in print.